Thermophysical Properties of Binary Aliphatic Quaternary Ammonium Ionic Liquids: TMPAFSAxTFSA1-x

Mizuhata, Minoru
Kunikata, Nobuaki
Deki, Shigehito

(Citation)
ECS Transactions,25(39):3-12

(Issue Date)
2010

(Resource Type)
journal article

(Version)
Version of Record

ECS Transactions, 25 (39) 3-12 (2010)
10.1149/1.3378967 ©The Electrochemical Society

Thermophysical Properties of Binary Aliphatic Quaternary Ammonium Ionic Liquids: $TMPAFSA_xTFSA_{1-x}$

Minoru Mizuhata, Nobuaki Kunikata, and Shigehito Deki

Department of Chemical Science and Engineering, Graduate School of Engineering, Kobe University 1-1 Rokkodai-cho, Nada, Kobe, 657-8501 Japan

The anionic binary Ionic liquids; $TMPAFSA_xTFSA_{1-x}$ were prepared as mixture of TMPATFSA and TMPAFSA. From the results of DSC analysis, the binary system showed the simple binary eutectic phase diagram and the eutectic point was found at the composition point of x = 0.33. In this system, each anion vibrated independently and showed isomerization equilibria displacement with temperature change. It was suggested that the equilibria displacements affected to the liquid structure and cis-trans isomerization of each anion played an important role in the solidification of $TMPAFSA_xTFSA_{1-x}$.

Introduction

Various kinds of ionic liquids have become an expanding topic of chemical research focusing their properties such as a negligible vapor pressure, nonflammability, and good ability to dissolve organic and inorganic compounds, and polymeric materials. Using these unique properties, ionic liquids are expected as next-generation superior media or solvents for various kinds of utilizations, for example, as environmentally friendly solvents for chemical synthesis, biocatalysis, separation technologies, and nanomaterial preparations. Especially the utilization of ionic liquids for the electrochemical devices such as rechargeable lithium batteries, fuel cells, electrochemical capacitors, electrodeposition, and so on have been focused and investigated [1-4].

Recently, ionic liquids including bis(fluorosulfonylamide)anion (FSA^-) have attracted much attention due to its higher conductivity and lower viscosity than ionic liquids including bis(trifluorosulfonyl-amide) anion ($TFSA^-$) [5, 6]. However, there are some criticisms of stability and higher melting points. With trimethyl-n-propylammoniumcation ($TMPA^+$), the melting point of TMPAFSA is 43.2 °C. It is higher than the melting point of TMPATFSA (19.8 °C). Consequently, we prepared the anionic binary ionic liquid namely $TMPAFSA_xTFSA_{1-x}$. Studies on conductivity and structure of the cationic binary ionic liquids have been reported in the literature [7-9]. So in this report, the anionic binary ionic liquid: $TMPAFSA_xTFSA_{1-x}$ was prepared as mixture of TMPAFSA and TMPATFSA which are as shown in Fig.1. The binary ionic liquid was prepared with a wide composition range in order to get the knowledge about the correlation of composition and properties, focusing cis-trans isomerization of FSA^- and $TFSA^-$ in the anionic binary system.

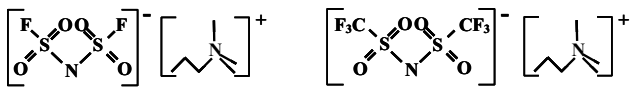

TMPAFSA TMPATFSA

Fig.1. Structural formulae of TMPAFSA and TMPATFSA.

Experimental

Sample Preparation

TMPAFSA and TMPATFSA were synthesized by an anion-exchange method under ambient atmospheric conditions [9]. Aliphatic quaternary ammonium halides were obtained based upon the reaction of *n*-Propyl bromide (above 95 %, Tokyo Kasei Kogyo Co., Ltd.) with trimethylamine (30 wt%, Nacalaitesque Inc.) as follows:

$$n\text{-}C_3H_7Br + (CH_3)_3N \longrightarrow n\text{-}C_3H_7(CH_3)_3NBr \quad (1)$$

n-Propyl bromide and excess of trimethylamine were mixed and stirred in acetone for 8 hr at 40 °C. The resulting salt was collected after evaporation and residual trimethylamine was removed with acetone until pure white salt of trimethyl-n-propylammonium bromide (TMPABr) was obtained. Then, to synthesize TMPAFSA and TMPATFSA, TMPABr was mixed with LiTFSA (Morita Chemical Industries Co., Ltd.) or KFSA (Dai-ichi Kogyo Seiyaku Co., Ltd) respectively for anion-exchange reaction as following equations.

$$n\text{-}C_3H_7(CH_3)_3NBr + KN(SO_2F)_2 \longrightarrow n\text{-}C_3H_7(CH_3)_3NN(SO_2F)_2 + KBr \quad (2a)$$

$$n\text{-}C_3H_7(CH_3)_3NBr + LiN(SO_2CF_3)_2 \longrightarrow n\text{-}C_3H_7(CH_3)_3NN(SO_2CF_3)_2 + LiBr \quad (2b)$$

LiTFSA or KFSA and equimolar amount of TMPABr were separately dissolved in distilled water in order to prepare the respective aqueous solutions. These solutions were mixed for 5 hr at 50 °C using magnetic stirrer. The mixed solution phase-separated into organic and aqueous phases. Then the organic phase was repeatedly refined with distilled water and 1,2-dichloroethane (99 %, Nacalai Tesque Inc.) until no residual byproducts such as KBr and LiBr exist in the medium. $AgNO_3$ (Nacalai Tesque Inc.) was used to check for the presence of LiBr. The recovered organic phase was dried under vacuum for 12 hr at 95 °C and then TMPAFSA and TMPATFSA were obtained. They were stored in a glove box under dry nitrogen atmosphere. To prepare the anionic binary ionic liquid: $TMPAFSA_xTFSA_{1-x}$, TMPAFSA and TMPATFSA were mixed with a wide composition range and stirred for 3 hr at 50 °C in the glove box.

Phase Transition Analysis

Phase transition points of ionic liquids were determined by the differential scanning calorimetry (DSC) measurement (Thermo Plus DSC 8230L of Rigaku Denki Co.) with a sample sealed in an aluminum pan. The employed temperature range of scanning was at least from -50 to 50 °C and the scan rate was 5 °C min^{-1}. Cooling and heating processes are repeated more than three times in dry N_2 gas flow.

Electrical Impedance Measurement

The electrical conductivity was measured by AC impedance measurement using a precision LCR meter (4284A and 4285A of Agilent Technology) with a 16452A test fixture in order to be applied on low conductive liquids[10,11]. The electrode area was 38 mm and the distance was 0.5 mm. The cell was calibrated by using a 0.01 M KCl aqueous solution at 25 °C. The temperature dependence of the conductivity was

measured within the temperature range at least from 40 to 60 °C and the VTF parameter are calculated from the temperature dependence using Gauss-Newton matrix operation method [12].

Viscometer

The dynamic viscosity was measured by a cone-plate digital viscometer (TVE-22L of Toki Sangyo Co., Ltd.). A cone rotor 1°34' × R24 was used and rotating speed was 5 rpm. From the obtained dynamic viscosity, the fluidity: ϕ was gained as the reciprocal of dynamic viscosity. The temperature dependence of the dynamic viscosities was measured and the VTF parameter was calculated using Gauss-Newton matrix operation method similar to conductivity determination.

Densimeter

The density was measured by a vibrating tube digital densimeter (DMA602 of Anton paar). The temperature dependence of the density was measured at the temperature range from at least 40 to 60 °C.

Raman Spectroscopy

Raman spectra were recorded by a triple spectrometer (T-64000 of Jobin Yvon/HORIBA) with a charge coupled device detector cooled with liquid nitrogen. The 532 nm line of a Nd^{3+}: YVO_4 laser (JUNO 532-100S of Showa Optronics Co., Ltd.) was used for excitation. A sample was loaded into a 5 mm diameter glass tube and set into the Raman cell (#2000-A of AABSPEC). Temperature was controlled with a digital temperature control system equipped with a K-type thermocouple. The spectral range was from 200 to 1000 cm^{-1} and the temperature range was from 40 to 120 °C.

Small and Wide Angle X-ray Scattering (SWAXS)

The liquid structure was investigated by SWAXS (SAXSess of Anton Paar) equipped with Kratky Camera optical arrangement. PW3830 laboratory X-ray generator with X-ray tube (CuKα, 1.542 Å, 40 kV and 50 mA) was used. The sample was loaded into quartz capillary by a syringe. The temperature range was from 60 to 120 ºC. The exposure time of X-ray was 20 minutes and detection was performed with the 2D imaging-plate reader (Perkin Elmer).

X-ray Diffraction (XRD)

XRD pattern was measured using X-ray generator (Rint-TTR of Rigaku Co., Ltd.) equipped with semiconductor detector and low temperature control unit (PTC30) which can operate step-by-step temperature controlling mode. The samples were investigated by focusing method with a Ni filter using rotating target (CuKα, 1.542 Å, 50 kV and 300 mA). A scanning speed of 4° min^{-1} was used within the range from 10 to 60°. Using the PTC30, we measured XRD patterns at every 20 °C as stepwise procedure between -100 °C and 50 °C and heating and cooling rates were 1 °C min^{-1}. At each measurement temperature, the sample was allowed to stabilize for 10 min before measurement. In order to confirm the effect of heat cycle, the stepwise procedure was repeated 9 times.

Results and Discussion

Thermal Analysis

A phase diagram of the binary system was gained as shown in Fig. 2 from the results of the phase transition analyses. At the phase transition points, the endothermic peak which corresponded to an enthalpy of fusion was observed for each sample. Excepting the systems of the single or eutectic salts, there were two endothermic peaks in the temperature range. These are shown in Fig. 3. They were assigned to the temperatures on the liquidus and solidus lines and were linked with each value on the phase diagram. From the phase diagram, it is indicated that $TMPAFSA_xTFSA_{1-x}$ showed the simple binary eutectic phase diagram composed of two kinds of immiscible crystals and completely miscible melt, and the eutectic point was found at the composition point of x=0.33. The eutectic point was confirmed at 5.5 °C and this is very lower value than the melting points of TMPAFSA and TMPATFSA; 43.2°C and 19.8°C, respectively.

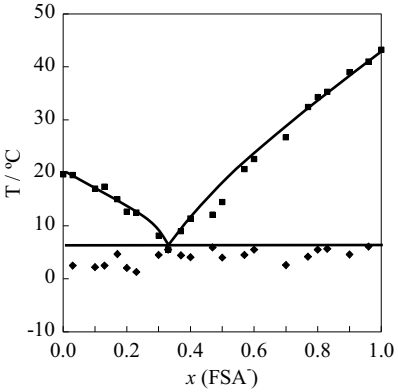

Fig. 2. Phase diagram of $TMPAFSA_xTFSA_{1-x}$.

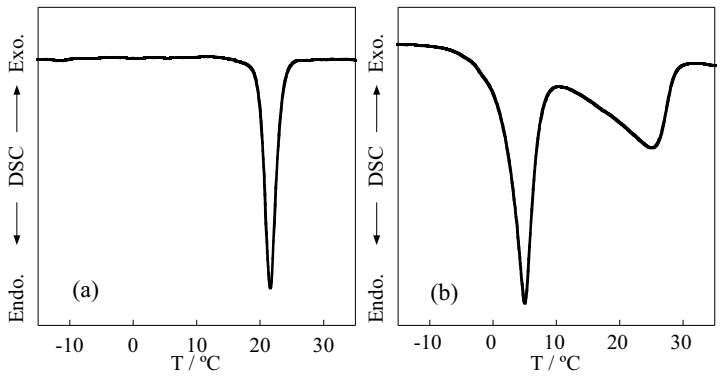

Fig. 3. DSC curves of (a) TMPATFSA and (b) TMPA $FSA_{0.70}TFSA_{0.30}$.

Conductivity and Viscosity

Fig. 4 represents composition dependence of conductivities and fluidities for $TMPAFSA_xTFSA_{1-x}$ at 60°C. On the whole compositions, it is confirmed that the conductivities and fluidities of $TMPAFSA_xTFSA_{1-x}$ increased by mole fraction increase of FSA^- due to the better mobility of the FSA system, however, the inflection points were found around x = 0.33. It is suggested that there are two areas in which one is FSA^- dominant and the other is $TFSA^-$ dominant in this composition range.

At each composition, temperature dependence of conductivities and fluidities showed obvious curvatures that could imply Vogel-Tamman-Fulcher (VTF) behavior as shown in Fig. 5 (a) and (b) respectively, and the each VTF parameters was

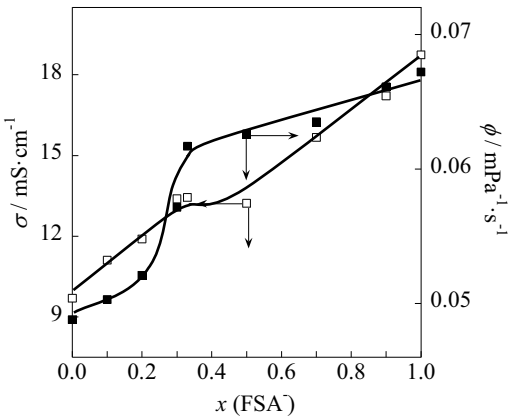

Fig.4. Composition dependence of conductivities and fluidities of $TMPAFSA_xTFSA_{1-x}$ at 60 °C.

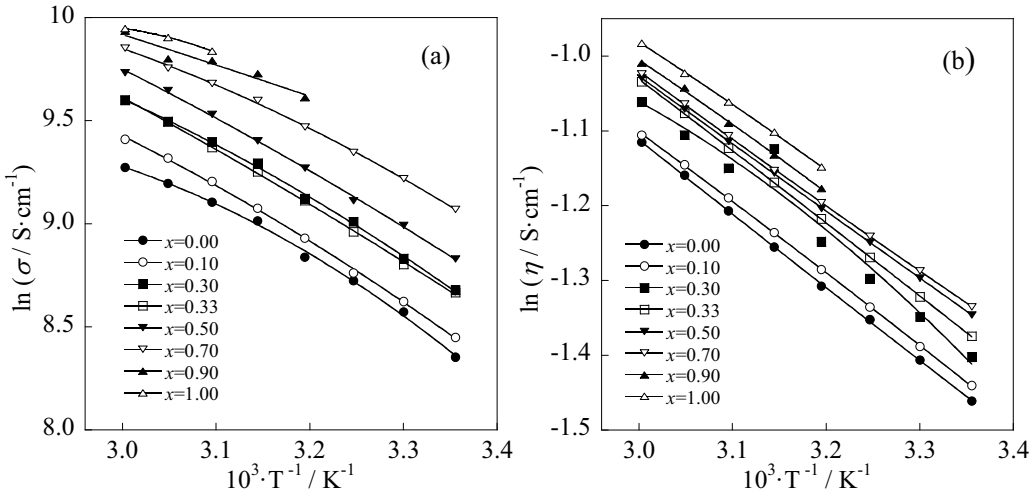

Fig. 5. Temperature dependence of (a)conductivities and (b)fluidities for $TMPAFSA_xTFSA_{1-x}$.

gained from the temperature dependence. VTF equation was given as following:

$$W = A\sqrt{T}\exp\left[-B/(T - T_0)\right] \quad (3)$$

where W is conductivity or fluidity and A, B and T_0 are constants. In the VTF parameter, the composition dependences of the $T_{0,\sigma}$ and $T_{0,\phi}$ of $TMPAFSA_xTFSA_{1-x}$ is shown in Fig. 6. Whereas $T_{0,\sigma}$ was constant at lower FSA contents ($0 < x < 0.33$), the value increased with the FSA content from the eutectic points as shown in Fig. 6. Cohen et al. proposed the following equation under constant pressure from a series of investigations about molecular movements and free volume[12-15].

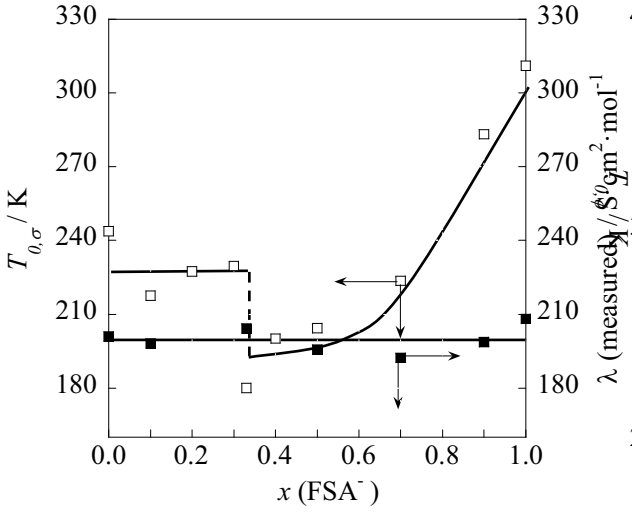

Fig. 6. Composition dependence of $T_{0,\sigma}$ and $T_{0,\phi}$ at 60 °C.

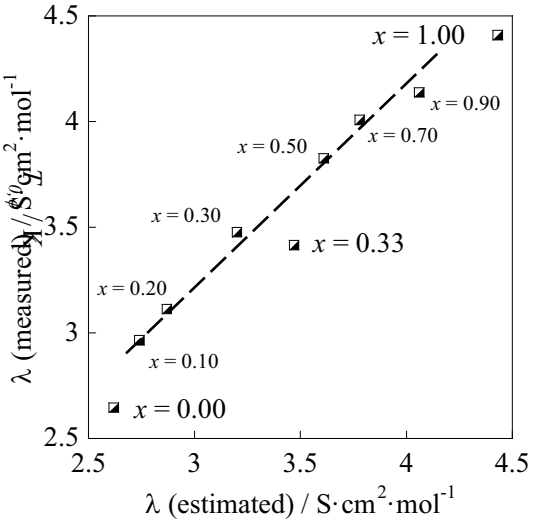

Fig. 7. Composition dependence of measured and estimated molar conductivities of $TMPAFSA_xTFSA_{1-x}$.

$$v_f = \alpha \bar{v}_m (T - T_0) \quad (4)$$

where v_f is free volume, α is coefficient of thermal expansion and $\bar{v}_m$ is mean molecular volume. Here, free volume means volume necessary for molecular movements and free volume vary in proportion to the difference between T_0 and measuring temperature. The value of $T_{0,\sigma}$ at the eutectic point was quite low (ca -100 °C), so, from this figure, it is suggested that the eutectic composition has the conductive space with lowest hindrance. On the other hand, composition dependence of $T_{0,\phi}$ showed constant value. This difference between $T_{0,\sigma}$ and $T_{0,\phi}$ was attributed to the difference in ionic movements between electrical conductance and fluidity, or in other words whether external electrical field gradient affects ionic movements or not. Fig. 7 represents the plots of the measured molar conductivities of $TMPAFSA_xTFSA_{1-x}$ as a function of the estimated molar conductivities which was obtained from empirical Walden's rule at 60 °C[16]. It is well known that the product of the viscosity and the equivalent ionic conductance at infinite dilution in electrolytic solutions is a constant under this rule and it is applicable for also a wide variety of ionic liquid [17,18]. Whereas plots of mixture compositions except for x = 0.33 was on the broken line but measured molar conductivity was only at x = 0.33; eutectic composition was lesser than the value on the line. It means measured molar conductivity at eutectic composition was lesser than the estimated value from the empirical Walden's rule using the results of viscosity measurement. It is indicated that the dissociation of the cation and anions in eutectic composition have a lesser degree of dissociation and have less free volume than the other mixture compositions.

Structure of Binary Salts at Liquid Phase

Fig. 8 indicates the results of Raman spectra of $TMPAFSA_xTFSA_{1-x}$ and TMPABr from 250 to 600 cm^{-1} at 60 °C. Many vibrations attributed to FSA^- and $TFSA^-$ appear in this spectral range and TMPABr represents Raman spectrum attributed $TMPA^+$. There were no significant shifts but only changes in peak intensities due to the abundance ratio of two anions. So it seems that the two different anions vibrate independently. Recently, Fujii et al. reported that the Raman spectra attributed to cis-trans isomerization of FSA^- and $TFSA^-$ was observed in this spectral range and these peaks changed the intensity ratio with changing temperature [6,19]. Fig. 9 indicates Raman spectra attributed to isomerization of FSA (cis- : 350 cm^{-1} and trans- : 360 cm^{-1}) and TFSA (cis- : 410 cm^{-1} and trans- : 400 cm^{-1}) of $TMPAFSA_xTFSA_{1-x}$ from 60 to 120 °C. In this temperature range, the intensity ratio of cis and trans isomer of each anion changed gradually with temperature change due to the isomerization equilibria displacement by the temperature change.

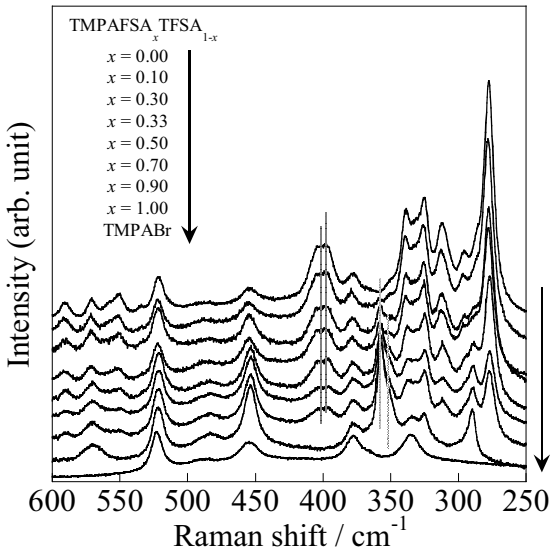

Fig. 8. Raman spectra of $TMPAFSA_x$ $TFSA_{1-x}$ at 60 °C.

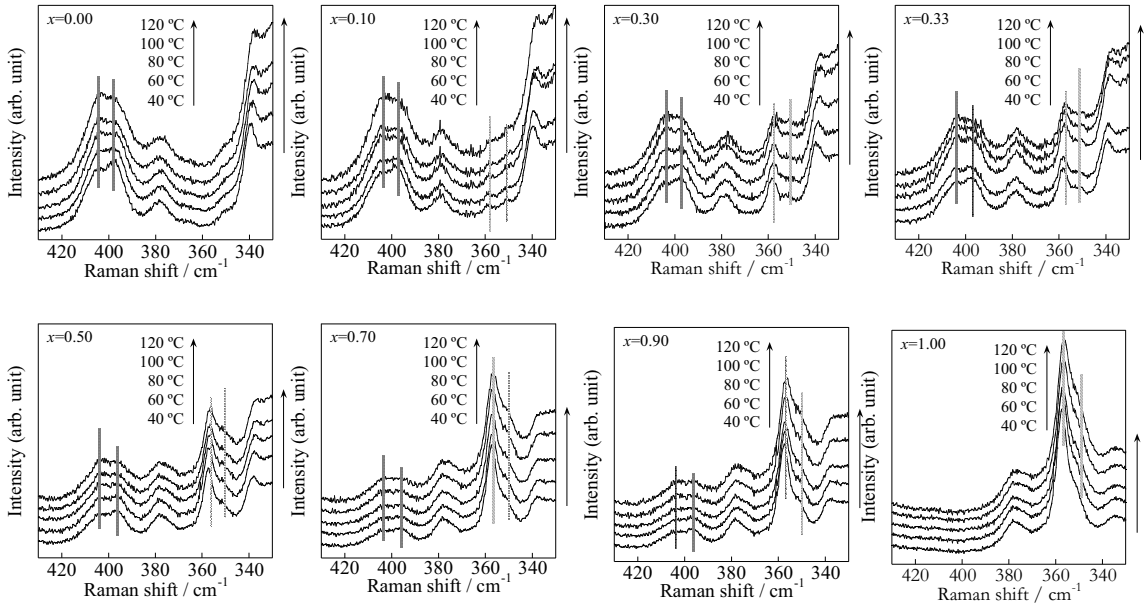

Fig. 9. Raman spectra of $TMPAFSA_xTFSA_{1-x}$ between 60 and 120 °C.

The SWAXS profiles of $TMPAFSA_xTFSA_{1-x}$ at 60 °C are shown in Fig. 10. The profile of quartz capillary is also shown in the figure. There are two significant halos (1st halo: q = ca. 8 nm^{-1} and 2nd halo : q = ca. 13 nm^{-1}). It is known that halo intensities reflects scattering factor and now, in this system, there are equilibria displacement between 60 °C and 120 °C and cis isomer ratio increased with temperature increase from the results of Raman spectroscopy. Therefore, the scattering factor of the sample was supposed to change due to equilibria displacement by temperature change. Fig. 11 represents the temperature dependences of the intensity ratio which was obtained by dividing the 1st halo by the 2nd halo. In this figure, the intensity ratio of only the sample

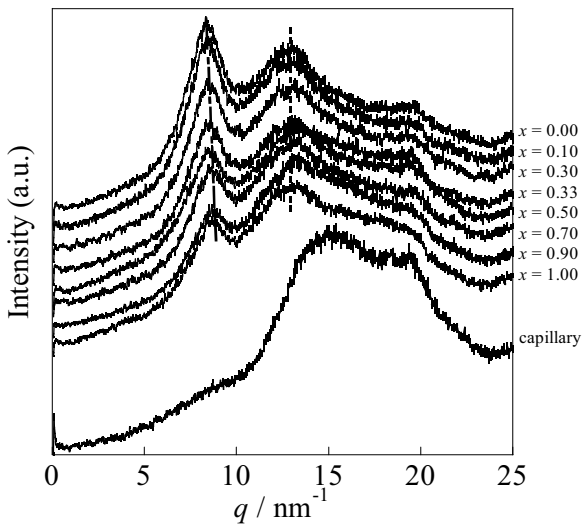

Fig. 10. SWAXS profiles of $TMPAFSA_xTFSA_{1-x}$ at 100 °C .

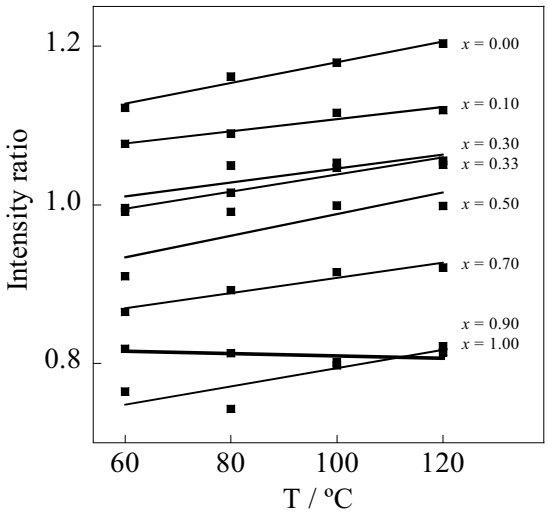

Fig. 11. Temperature dependence of intensity ratio of $TMPAFSA_xTFSA_{1-x}$.

at x = 1.00 was almost a constant value between 60 °C and 120 °C. This result could come from the different influences from the equilibria displacement of FSA^- and $TFSA^-$. FSA^- and $TFSA^-$ possess cis-trans isomerization by intramolecular rotation and the effect of intramolecular rotation of $TFSA^-$ to surrounding ions is supposed to be more drastic than that of FSA^- due to the bulkiness of $TFSA^-$. The temperature dependence of the intensity ratio is constant in the range of 60 to 120 °C for the composition of the sample at x=1.00 (TMPAFSA) which consisted of only FSA^- although there is equilibria displacement.

Structure of Binary Salts at Supercooled and Solid State

Although we successfully gained the phase diagram, we can obtain only thermal behavior and little information about solid state structure from just the results of DSC. So in this study, we discuss the solid state structure of $TMPAFSA_xTFSA_{1-x}$ with XRD as a stepwise procedure.

From the results of XRD patterns on cooling process at 6th step as shown in Fig. 12, sample at x = 0.00 was hard to solidify and remained in a supercooled state until -100 °C despite TMPATFSA having a melting point at 19.8 °C. On the other hand, sample at x = 1.00 which has melting point at 43.2 °C also tend to get supercooled state but to a lesser extent. It is considered that this difference was attributed to the degree of effect to the surroundings which was presented by intramolecular rotation under supercooled state. The effect by intramolecular rotation of $TFSA^-$ is supposed to be more drastic due to its bulkiness than FSA^- from the results of SWAXS, so it makes the solidification of TMPATFSA unsettled. Interestingly, the sample at x = 0.33 hardly supercooled although it contain TMPATFSA. It is suggested the mixture composition of one-third TMPAFSA and two-thirds TMPATFSA is very stable for this system.

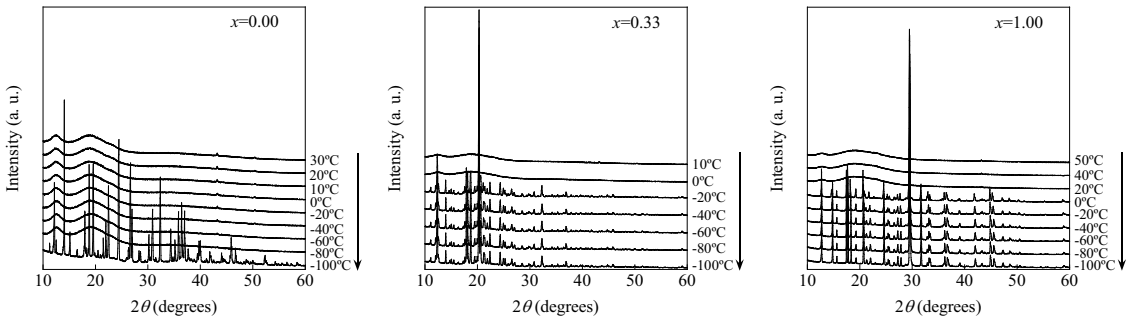

Fig. 12. XRD patterns of $TMPAFSA_xTFSA_{1-x}$ under 6th cooling process.

Fig. 13 represents the XRD patterns of each composition at -100 °C in each step. It is obvious that the sample at x = 0.00, which is hard to solidify, showed different XRD patterns at each step. It was suggested that the various stable solid phases exists under the melting point, and the phase transition was not fixed clearly by the varieties of the molecular conformation. On the other hand, XRD patterns appeared at relatively same angle for x = 1.00. Such a discrepancy may also be due to the differences of effects to surroundings by isomerization of both FSA^- and $TFSA^-$ under supercooled state. Eutectic mixture also showed XRD patterns at relatively same angle, hence, the bulkiness of $TFSA^-$ might be suppressed in the eutectic composition. In the figure, XRD patterns of x

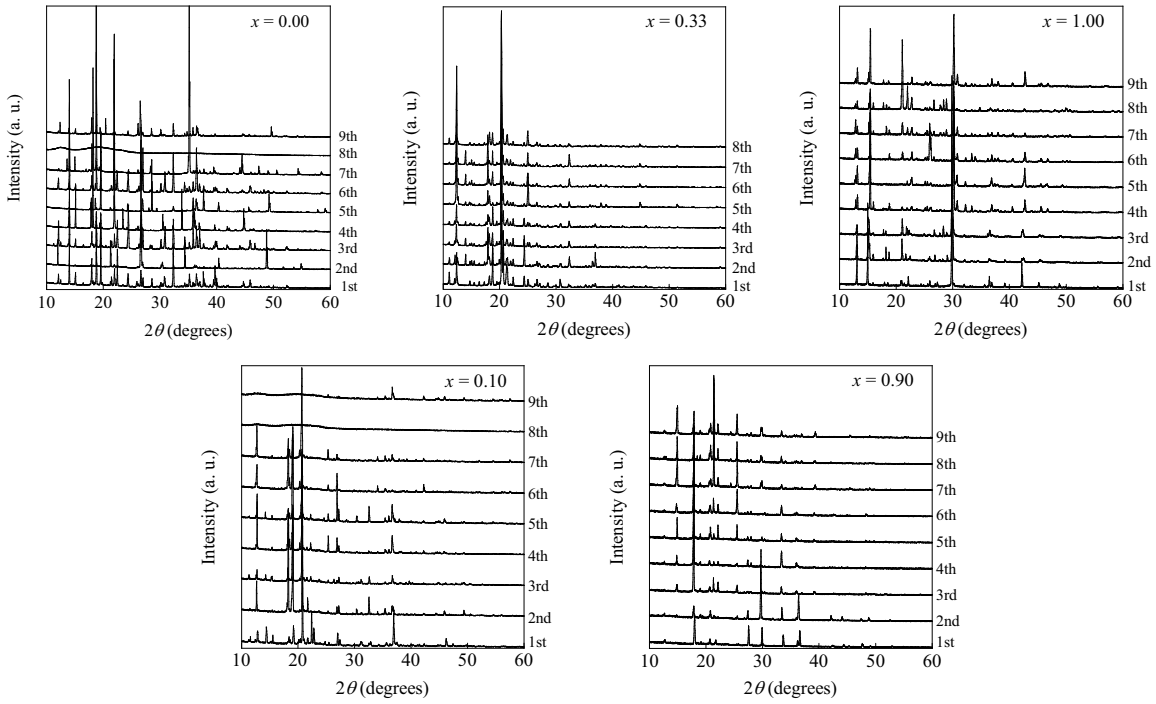

Fig. 13. XRD patterns of $TMPAFSA_xTFSA_{1-x}$ at -100 °C of each step.

= 0.10 and x = 0.90 were gained at relatively same angle. However, the base lines of x=0.10 exhibited a wavy like nature, whereas x=0.90 had no such base lines. It is attributed to the fact that, at cooling process, these compositions passed over liquidus and solidus line in the side of TMPATFSA and TMPAFSA each other.

Conclusions

$TMPAFSA_xTFSA_{1-x}$ showed the simple binary eutectic phase diagram and the eutectic point was 5.5 °C at the composition of x = 0.33. The electrical conductivity and fluidity was investigated using the empirical Walden's rule and it was suggested that efficiency of ion deviation at eutectic composition was specific. In the system, each anion in the binary system vibrated and showed cis-trans isomerization independently, and the cis isomer ratio increased with the temperature increase. From the results of SWAXS, it is suggested that intramolecular rotation of $TFSA^-$ affects to surroundings drastically due to its bulkiness and that of FSA^- is more moderate. The results of XRD measurement indicated that TMPATFSA was much harder to solidify than TMPAFSA and tend to solidify as different crystal in each stepwise procedure. This may come from the bulkiness of $TFSA^-$. Therefore, effects to surroundings from cis-trans isomerization by intramolecular rotation play an important role on the solidification of $TMPAFSA_xTFSA_{1-x}$ which consisted of complicated ions.

Acknowledgments

This study was supported by Grant-in-Aid for Scientific Research (No. 17073017) "Science of Ionic Liquids" from MEXT of Japan.

References

1. N. Nakagawa, S. Izuchi, K. kuwana, T. Nukuda, and Y. Aihara, *J. Electrochem. Soc.* , **150**, A695 (2003).
2. Z-B.Zhou, H. Matsumoto, and K. Tatumi, *Chemistry-A.Euro. J.* , **12**, 2196 (2006).
3. A. Noda, M. A. B. H. Susan, K. Kudo, S. Mitsushima, K. Hayamizu, and M. Watanabe, *J. Phys. Chem. B*, **107**, 4024 (2003).
4. E. Paillard, Q. Zhou, W. A. Henderson, G. B. Appetecchi, M. Montanino, and S Passerini, *J. Electrochem. Soc.*, 156, A891 (2009).
5. H. Matsumoto, H. Sakaebe, K. Tatsumi, M. Kikuta, E. Ishiko, and M. Kono, *J. Power Sources*, **160**, 1308 (2006).
6. K. Fujii, S. Seki, S. Fukuda, R. Kanzaki, T. Takamuku, Y. Umebayashi, and S. Ishiguro, *J. Phys. Chem. B*, **111**, 12829 (2007).
7. M. Mizuhata, K. Yaso, Y. Ito, and S. Deki, *Electrochemistry*, **73**, 606 (2005).
8. M. Mizuhata, M. Maekawa, and S. Deki, *ECS Transactions*, **3**(35), 89 (2007).
9. M. Mizuhata, T. Minowa, M. Maekawa, and S. Deki, *ECS Transactions*, **16(49)**, 69 (2009).
10. A. K. Jonscher, *J.Mater. Sci*., **13**, 553 (1978).
11. N. E. Hill, W. E. Vanghan, A. H. Pricd and M. Davies, Dielectric properties and molecular behavior, p. 49, van Norstrand Reinhold, London (1969)
12. C. A. Angell, *J. Phys. Chem*., **68**, 1917 (1964).
13. M. H. Cohen and D. Turnbull, *J. Chem. Phys.*, **31** 1164 (1959).
14. D. Turnbull and M. H. Cohen, *J. Chem. Phys.*, **34** 120 (1961).
15. D. Turnbull and M. H. Cohen, *J. Chem. Phys.*, **52**, 3038 (1970).
16. P. Walden, *Z.Phys. Chem.*, **157**, 389, (1931).
17. Z-B.Zhou, H. Matsumoto, and K. Tatumi, *Chem. Eur. J.* , **10**, 6581 (2004).
18. Y. Yoshida, K. Muroi, A. Otska, G. Saito, M. Takahashi, T. Yoko, *Inorg. Chem*., **43**, 1458 (2004).
19. K. Fujii, T. Fujimori, T. Takamuku, R. Kanzaki, Y. Umebayashi, and S. Ishiguro, *J. Phys. Chem. B*, **110**, 8179 (2006).